Journal of The Electrochemical Society, 2025 **172** 010501

Low-Concentration Electrolyte Design for Wide-Temperature Operation in Sodium Metal Batteries

Qipeng Zhang,[=,z] Xin Wang,[=] Hao Li, and Rui Qiao[z]

Department of Mechanical Engineering, Virginia Polytechnic Institute and State University, Blacksburg, Virginia, 24060, United States of America

Sodium metal batteries (SMBs) are cost-effective and environmentally sustainable alternative to lithium batteries. However, at present, limitations such as poor compatibility, low coulombic efficiency (CE), and high electrolyte cost hinder their widespread application. Herein, we propose a non-flammable, low-concentration electrolyte composed of 0.3 M $NaPF_6$ in propylene carbonate (PC), fluoroethylene carbonate (FEC), and 1,1,2,2-tetrafluoroethyl 2,2,3,3-tetrafluoropropyl ether (TTE). This low-concentration electrolyte not only reduces cost but also delivers rapid ion diffusion and superior wetting properties. While the Na||$FePO_4$ system with this electrolyte demonstrates slightly reduced performance at room temperature compared to standard-concentration formulations (S-PFT), it excels at both high (55 °C) and low (−20 °C) temperatures, showcasing its balanced performance. At 0.5 C (charge)/1 C (discharge), capacity retention reaches 92.8% at room temperature and 98.5% at elevated temperature, with CE values surpassing 99% and 99.63%, respectively, and significant performance sustained at −20 °C at 0.2 C. This electrolyte development thus offers a well-rounded, economically viable path to high-performance SMBs for diverse environmental applications.

 [DOI: 10.1149/1945-7111/ada372]

Manuscript submitted October 28, 2024; revised manuscript received December 16, 2024. Published January 2, 2025.

Supplementary material for this article is available online

Electric vehicles and electric grids powered by renewable, but typically intermittent energy sources demand low-cost, high-performance electrochemical energy storage technologies. Due to their high energy density and stability, lithium metal batteries (LMBs) currently hold a leading position in meeting this demand. However, LMBs are expensive and largely infeasible for grid-scale energy storage applications due to a lack of lithium (approximately 0.0065% in the Earth's crust). Hence, it is critical to develop alternative battery technologies. Sodium metal batteries (SMBs) are gaining popularity due to their low cost ($50–100 kWh^{-1}), and abundant sodium (around 0.048% in the Earth's crust).[1–3]

The performance of SMBs, however, is still far from ideal in large part due to limited research in sodium-based chemistry.[4–6] Current research on SMB focuses on electrolyte and electrode materials, as well as interactions between electrode and electrolyte.[7–9] In particular, electrolytes in SMBs are a crucial element that influences the electrochemical window, energy density, and properties of the electrode/electrolyte interfaces. However, the mainstream organic electrolytes for SMBs suffer from flammability, low thermodynamic stability, and toxicity.[8,10] Indeed, it remains a great challenge to create SMB electrolytes that are non-flammable, thermodynamically stable, and eco-friendly.

In developing SMB electrolytes, much effort has been dedicated to introducing flame retardants, inert diluents, and ionic liquids to address the limitations of existing electrolytes.[11–13] For instance, Chang et al. developed a 0.5 M NaTFSI-incorporated MBP-ionic liquid electrolyte to replace conventional organic electrolyte, and at a rate of 1 C, the Na||$NaFePO_4$ cell demonstrated steady cycling performance with 65% capacity retention.[14] Zhang et al. proposed a non-flammable electrolyte containing NaFSI-triethyl phosphate (TEP)/1,1,2,2-tetrafluoroethyl-2,2,3,3-tetrafluoropropyl ether (TTE) (1:1.5:2 in mole), in which the Na|| $NaCu_{1/9}Ni_{2/9}Fe_{1/3}Mn_{1/3}O_2$ (Na-CNFM) with a coulomb efficiency (CE) of 99.8%–99.9% over 100 cycles at 0.2 C.[11] These studies effectively tackle some key limitations of standard electrolytes, but they are generally restricted to room temperature, although an ideal SMB electrolyte should work in a wide temperature range. As such, new strategies are needed in the development of SMB electrolytes.

Previous works on wide-temperature SMBs generally focused on applying standard or high-concentration salts to improve the wide-temperature performance. Wu et al. designed sodium bis(trifluoromethylsulfonyl)imide (NaTFSI) in N-methyl-N-propylpyrrolidiniumbis(fluorosulfonyl)imide ([Py_{13}][FSI]) and 1,2-bis (1,1,2,2-tetrafluoroethoxy) ethane (TFEE) (1:3:1 by molar ratio, ∼1.15 M). These dedicated electrolytes showed outstanding long-term cycling performance with a capacity retention of 95.5% at 5 C after 2000 cycles at 25 °C, CE of ∼99% after 240 cycles at 60 °C, and specific capacity of 132 mAh g^{-1} achieved by the NFM||Na cell at −20 °C.[15] Similarly, Chou et al. introduced succinonitrile (SN)-based electrolyte containing $NaClO_4$/SN/1,3,2-dioxathiolane-2,2-dioxide (DTD) (∼2 M), which delivered a capacity retention of 82.8% after 800 cycles (25 °C) and 86.3% after 100 cycles (60 °C).[16] However, given that the Stokes radius and de-solvation energy of Na^+ are less than those of Li^+.[17,18] We hypothesize that it is possible to maintain acceptable even better performance from SMBs with low-concentration electrolytes even at wide temperatures.

To verify the above hypothesis, we report an electrolyte consisting of 0.3 M (hereafter refered to as L-PFT)/1.0 M (as reference group, S-PFT) $NaPF_6$ dissolved in a mixture of propylene carbonate (PC), Fluoroethylene carbonate (FEC), and 1,1,2,2-tetrafluoroethyl 2,2,3,3-tetrafluoropropyl ether (TTE) (3:3:4 by volume). This well-designed electrolyte exhibits non-flammability, high compatibility with both Na metal anode and cathode as well as better electrochemical performance. Benefiting from this electrolyte, the as-developed Na||$FePO_4$ battery delivered a capacity retention of 94.8% at 0.5 C (charge)/1 C (discharge) with a very high CE of 99.88% over 350 cycles for S-PFT. The reduced conductivity of L-PFT still affords acceptable capacity retention and CE, which are 2% and 0.46% lower than those of S-PFT. The cells with L-PFT showed capacity retention of 90.8% even at a high rate of 2 C after 500 cycles. Surprisingly, the cell performs with L-PFT at temperatures of 55 °C better than S-PFT due to $NaPF_6$ decomposition, the problem of thermodynamic stability is thus the main one to take into account at high temperatures compared to the room temperature. Furthermore, the low viscosity, rapid diffusion rate, and improved wetting performance of the battery with L-PFT allow for significant performance at low temperatures (−20 °C). The present electrolyte

[=]Equal contribution.
[z]E-mail: qipengzhang@vt.edu; ruiqiao@vt.edu

design, in our opinion, offers a fresh approach to improve the viability of SMBs technology, particularly concerning its coulombic efficiency, capacity performance, and compatibility.

Results and Discussion

Design and reveal solvation structures in two electrolytes.— Figure 1a illustrates the design strategy for our electrolyte. By varying the ratio of different salts, we modulate the interactions between Na^+ ions and solvents, which, in turn, influence the electrolyte's physical properties and interfacial behavior, thereby affecting its electrochemical performance. Specifically, $NaPF_6$ sodium salts were selected for their outstanding electrical conductivity and strong electrochemical stability. Propylene carbonate (PC) is employed as a solvent for dissolving sodium salts, known for its good conductivity. Indeed, 1.0 M $NaPF_6$ in PC is a SMB electrolyte. However, this electrolyte is associated with elevated interfacial impedance at Na metal anodes and accompanied by the continuous growth of electrolyte/electrode interphase. Recent studies have identified fluoroethylene carbonate (FEC) as a cosolvent (or additive), where its preferential defluorination generates an interphase rich in NaF, significantly enhancing the stability of metallic Na.[19–21] Despite these improvements, the electrolyte composed of 1.0 M $NaPF_6$ in FEC/PC still exhibits substantial flammability, as demonstrated in **Movie S1**, posing significant safety concerns for practical applications.

To address the issue of thermal stability, we introduced 1,1,2,2-tetrafluoroethyl 2,2,3,3-tetrafluoropropyl ether (TTE), a highly fluorinated ether. Recognizing that the inclusion of TTE may impact initial conductivity, a balanced approach was employed. To optimize both thermal stability and conductivity, we developed an electrolyte formulation of 1.0 M $NaPF_6$ in a PC: FEC: TTE mixture with a volumetric ratio of 3:3:4, designated as S-PFT. This formulation demonstrates high conductivity, an inorganic-derived interphase, and nonflammability, as depicted in **Movie S2**. In comparison to S-PFT, the L-PFT electrolyte, with a reduced salt concentration of 0.3 M, exhibits faster sodium ion diffusion, an organic-based interphase, and improved wetting performance, allowing L-PFT to maintain competitive performance characteristics while enhancing the overall safety profile of the electrolyte.

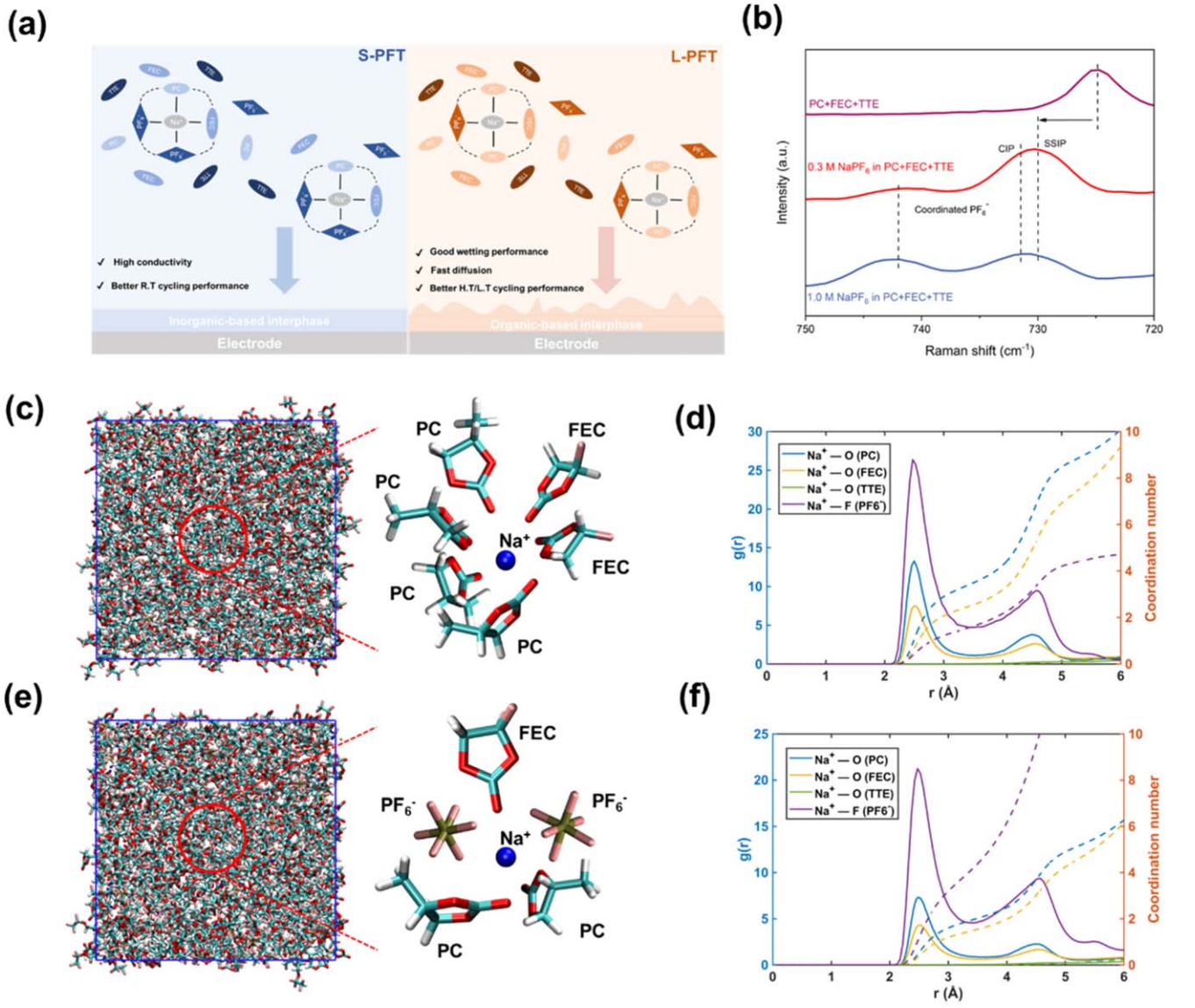

Figure 1. Design and solvation structure of 0.3 M and 1.0 M $NaPF_6$ in PC:FEC:TTE (3:3:4 vol%) electrolytes. (**a**) 0.3 M and 1.0 M mixed electrolytes design principle. (**b**) Raman spectra of 0.3 M and 1.0 mixed electrolyte and pure mixed solvents. (**c, e**) Snapshots of 0.3 M (c) and 1.0 M (e) electrolytes, along with their representative solvation structures. (**d, f**) Radial distribution functions Na atoms in 0.3 M (d) and 1.0 M electrolytes (f). The dashed lines are the integrated radial distribution function for the coordination number of O and F around Na^+ (dashed lines).

Electrolytes formulated with various solvents, sodium salts, and salt concentrations can result in substantial alterations in the Na^+ solvation structure. These changes can influence the interfacial composition and impact the plating/stripping behavior, thereby significantly affecting the overall electrochemical performance. To elucidate the solvation structure of the designed electrolytes, we conducted Raman spectroscopy experiments, as shown in Figs. 1b and S1 (**Supporting Information**). The peak observed in the 710–730 cm^{-1} region, a distinct feature in this spectral range, was analyzed to identify the different states of the C=O breathing bond on the carbonate ring in propylene carbonate (PC) and fluoroethylene carbonate (FEC).[22,23] Upon introducing $NaPF_6$ salt into these solvents, the peak shifted to a higher wavenumber, indicating an interaction between the salt and solvent molecules. Additionally, a new peak emerges at 742 cm^{-1}, which corresponds to the coordinated PF_6^- within the electrolyte.[24] In contrast, when $NaPF_6$ was utilized as the solute in TTE, no significant peak shift was observed, suggesting a negligible interaction between Na^+ and TTE.

The above observation is further corroborated by the Raman spectra of mixed solvents with varying $NaPF_6$ concentrations, where distinct peak blueshifts were detected as the salt concentration increased to 0.3 M. At a high salt concentration of 1.0 M, the peak at 731 cm^{-1}, associated with solvent-separated ion pairs (SSIP) and contact ion pairs (CIP), exhibited a further blueshift, reflecting the formation of these ion pairs in different proportions. Notably, the L-PFT electrolyte exhibited a higher proportion of SSIP relative to CIP compared to S-PFT, alongside a reduced fraction of coordinated PF_6^- (742 cm^{-1}). These comparative results indicate that the interaction between PF_6^- and Na^+ diminishes progressively from S-PFT to L-PFT, with the strongest interaction observed in S-PFT. The relative distance (d) between PF_6^- and Na^+, where a greater distance signifies a weaker interaction, is used here as a qualitative measure of the PF_6^-/Na^+ interaction strength. This analysis is supported by variations in the chemical bonds within the electrolyte components, as reflected in the Raman spectra. Consequently, the relative distances between PF_6^- and Na^+ follow the sequence: S-PFT (d_1) < L-PFT (d_2).

To further ascertain the solvation structure inferred from the above measurements, molecular dynamics (MD) simulations (see Fig. S2) were performed for L-PFT and S-PFT electrolytes. Figures 1c–1f and S2 display snapshots of the MD systems for these electrolytes as well as the coordination numbers and radial distribution functions (RDFs) for L-PFT and S-PFT. Figure 1d shows that, in L-PFT, PC, FEC, PF_6^- participate in Na^+'s first solvation shell, while TTE does not, which is consistent with the previous study.[11] In L-PFT, PC and FEC solvents dominate Na^+ ion's solvation shell: the total coordination number by solvent is 6.1 (3.5 PC and 2.6 FEC) and there is a small coordination contribution from PF_6^- (1.6 F atoms). In S-PFT (see Fig. 1f), the total number of coordination solvent molecules decreases from 6.1 to 3.6, with 2 PC and 1.6 FEC, while the coordination by anions' F atoms in anions increases from 1.6 to 4.6. This trend indicates that, as the concentration of $NaPF_6$ increases, PF_6 anions are more engaged in the solvation sheath and solvents are gradually depleted.

From MD trajectories, we can also delineate the molecular state of Na^+ ions in L-PFT and S-PFT. Ions in an electrolyte can be categorized into three populations with different solvation states: solvent-separated ion pairs (SSIPs), contact ion pairs (CIPs), and aggregates (AGG).[25,26] As shown in Fig. S13, in L-PFT, the majority (57.9%) of Na^+ ions are dissociated (SSIP); in S-PFT, the fraction of SSIP Na^+ ions decreases to 38.1% while that of AGG increasing from 18.6% to 39.8%. Physically, increased concentration leads to stronger screening of electrostatic repulsion between cations or anions and thus allows them to come closer to form AGG. The MD simulations further indicate that the efficient assembly of a PF_6 anion-based structure in S-PFT promotes the formation of an inorganic-rich interphase, attributed to an increased ratio of CIPs and AGG. In contrast, L-PFT forms solvent-derived structures, aligning well with the trends observed through Raman spectroscopy. This concordance between MD simulation results and experimental Raman data supports the validity of the proposed solvation structures.

Performance of designed electrolyte at room temperature.—We assembled Na||$FePO_4$ cells to evaluate the impact of the designed electrolytes on cycling behavior, with $FePO_4$ obtained through the de-lithiation of $LiFePO_4$ (further details in Fig. S3). As illustrated in Fig. 2a, the initial discharge capacity of the cell with S-PFT electrolyte is 144.6 mAh g^{-1}. Furthermore, S-PFT demonstrates remarkable cyclability, with a capacity retention of 94.8% and an average coulombic efficiency (CE) of 99.88% after 350 cycles at a charge rate of 0.5 C and a discharge rate of 1.0 C. However, as shown in Fig. S4, L-PFT, despite its lower viscosity (3.09 mPa·s), superior wetting performance (Fig. S5), and faster diffusion rate (Fig. S6), exhibits a slight reduction in performance, with capacity retention and CE being 2% and 0.46% lower, respectively, than those of S-PFT. Nevertheless, the performance of L-PFT remains significantly superior to that of traditional PC-based electrolytes, which exhibit a near-zero discharge capacity after 150 cycles, and also outperforms other reported electrolytes in the literature. (Figure S7 and Table S1).

The rate capability of the cells was also evaluated at different C-rates (Fig. 2b). While S-PFT exhibited the best performance with high C-rates, L-PFT delivered acceptable performance. The voltage profile of Na||$FePO_4$ cells with L-PFT demonstrates stable discharge capacities of 135.5, 123.7, 109.9, 98.3, 84.7, 65.0, and 47.3 mAh g^{-1} at rates of 0.1 C, 0.2 C, 0.5 C, 1.0 C, 2.0 C, 5.0 C, and 10 C, respectively. Two voltage plateaus of the voltage profile at approximately 3.2 V and 3.25 V are observed during the charge process (Fig. 2c), corresponding to the two-phase reaction from $NaFePO_4$ to $Na_{2/3}FePO_4$ and the solid solution reaction from $Na_{2/3}FePO_4$ to $FePO_4$, respectively.[27,28] During discharge process, a single plateau at 2.7 V is consistent with the results obtained from cyclic voltammetry testing (Fig. S8). It is noteworthy that the hysteresis between the charge-discharge voltage plateaus of $NaFePO_4$ is larger than that observed for $LiFePO_4$ (Fig. S9), likely due to the higher energy difference during phase transitions, slower intercalation kinetics, and greater charge transfer resistance for Na^+ ions compared to Li ions. Additionally, L-PFT cells also maintained a capacity retention of 90.8% after 500 cycles at a 2 C rate, indicating that L-PFT can support long-term, high-rate cycling (Fig. S10).

Electrode interphase evolution was investigated using electrochemical impedance spectroscopy (EIS) after extended cycling (Fig. 2d). The electrolyte resistance (R_s) was derived from the intercept of the high-frequency response with the real axis. Semicircles observed at mid-to-high frequencies represent the charge transfer resistance (R_{ct}) in the electrode-electrolyte interphases and the interfacial resistance ($R_{interphase}$) of the passivation surface layer, with the total cell resistance defined as $R_{cell} = R_{ct} + R_{interphase}$.[29,30] Notably, the S-PFT cell exhibited an R_s of 7.89 Ω and an R_{cell} of 152.14 Ω, whereas the L-PFT cell showed higher values, with R_s at 8.78 Ω and R_{cell} at 201.72 Ω.

X-ray photoelectron spectroscopy (XPS) was employed to further investigate the differences in interphase composition. The C 1 s spectrum reveals a C–C peak at 284.8 eV, indicative of conductive carbon, and a C–F peak at 291.2 eV, associated with FEC, indicating partial decomposition of FEC and its participation in interphase formation. The C–O (286.8 eV) and C=O (287.2 eV) peak in the C 1 s spectrum, alongside the C=O (531.4 eV) and C–O (533.1 eV) peaks in the O 1 s spectrum, are attributed to the decomposition of PC and FEC. The O 1 s peak at 536.5 eV corresponds to the decomposition of $NaPF_6$, resulting in PO_xF_y species.[31] The F 1 s and Na 1 s spectra indicate the presence of Na-F, which is essential for interphase formation. In L-PFT cells, the peak intensities for organic components (C and O-based elements) are higher, while those for inorganic components (e.g., Na-F) are lower. In contrast, MD simulations indicate that in S-PFT cells, an elevated salt concentration results in a 22.1% increase in the CIP ratio and a 39.8% increase

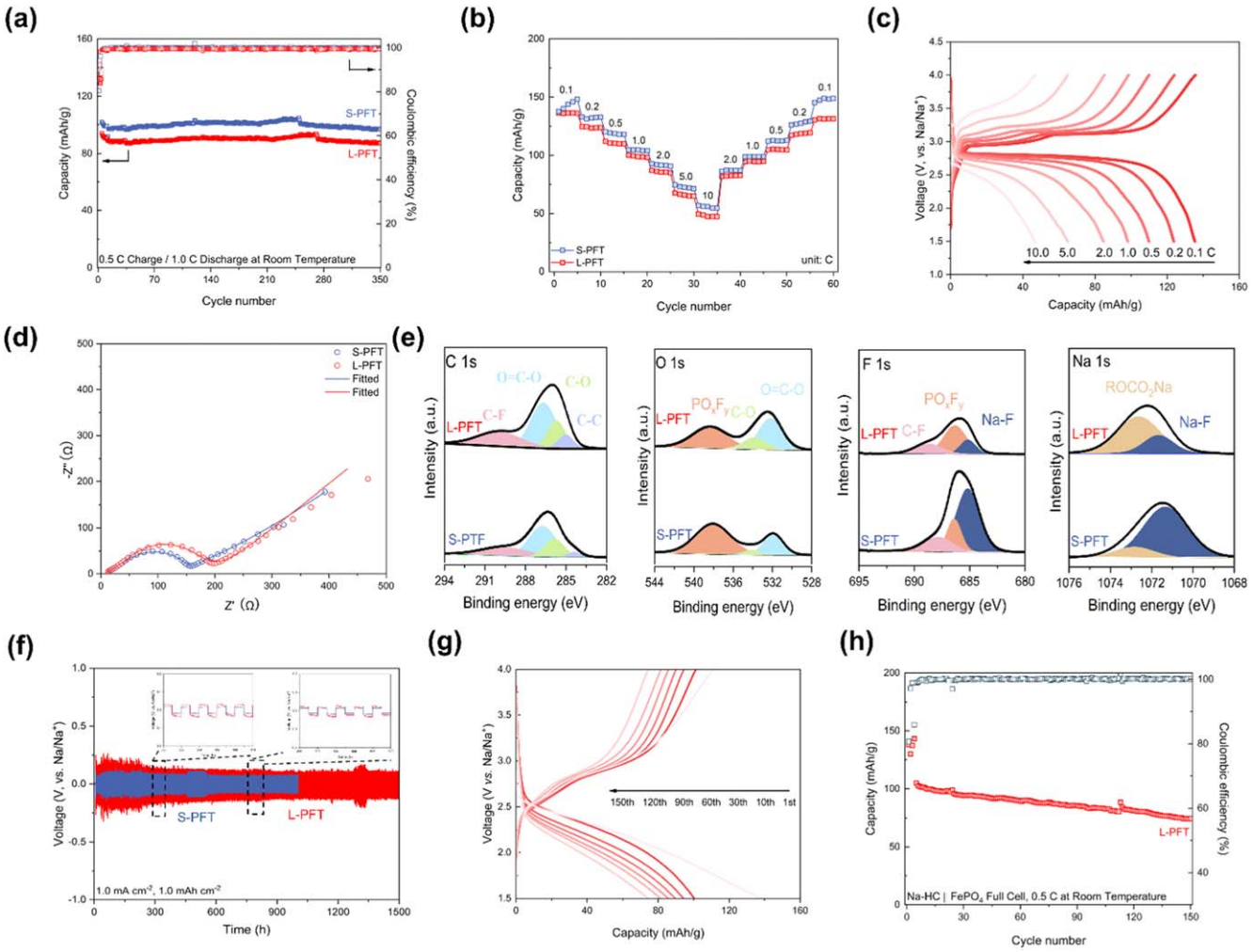

Figure 2. Electrochemical behavior of Na||$FePO_4$ cells. (a) Cycling performance of the Na||$FePO_4$ cells with two electrolytes at 0.5 C charge/1.0 C discharge. Rate performance of batteries (b) corresponding to voltage profiles with 0.3 M electrolyte (c). (d) EIS results for S-PFT (1.0 M) and L-PFT (0.3 M) after long cycles. (e) XPS spectra of cycled batteries: C 1 s, O 1 s, F 1 s and Na 1 s. (f) Na||Na symmetric cells using S-PFT and L-PFT electrolytes at 1.0 mA cm^{-2} with a cut-off capacity of 1.0 mAh cm^{-2}. (h) Voltage profiles of Na-HC||$FePO_4$ full cells with L-PFT(g). Cycling performance of the full cell at 0.5 C.

in the AGG ratio. This enhancement promotes greater coordination between PF_6^- and Na^+ ions, facilitating the formation of an anion-derived interphase. This configuration lowers the de-solvation energy of sodium ions and enhances Na^+ transfer through the interphase, due to the low Na^+ diffusion barrier of inorganic components, thereby improving cycling performance. These findings are consistent with the results from MD simulations, cyclic performance, and EIS measurements.

Further evidence of interphase differences was obtained by testing Na||Na symmetric cells at a current density of 1.0 mA cm^{-2} and an areal capacity of 1.0 mAh cm^{-2} (Fig. 2f). For the S-PFT electrolyte, the voltage hysteresis remained constant at ~70 mV after 1000 h, attributable to the formation of an inorganic-based interphase. In contrast, L-PFT exhibited an initial overpotential of ~170 mV, which stabilized at ~100 mV after 1500 h, with minimal fluctuations. This behavior is attributed to the formation of a flexible interphase with a low shear modulus, which can accommodate sodium metal expansion.[32,33] Consequently, even when the solvent-dominated interphase is less effective at preventing dendritic growth, the voltage hysteresis remains relatively stable compared to S-PFT.

To demonstrate the practical applicability of L-PFT, a full cell with hard carbon pre-embedded with limited sodium was assembled, replacing sodium metal. As shown in Figs. 2g–2h, a pre-cycle at 0.1 C was conducted to optimize the electrode/electrolyte interphase before long-term cycling at 0.5 C. The full cell exhibited a reversible discharge capacity of ~75 mAh g^{-1} at 0.5 C after 150 cycles. These results suggest that L-PFT is a promising electrolyte for the development of high-performance SMBs.

Performance of the designed electrolyte at high temperature (55 °C).—The high-temperature applicability of the designed electrolyte was investigated. Figure 3a shows a high initial coulombic efficiency using the L-PFT of ~ 72% at 55 °C, which is greater than the S-PFT (~ 68%). This result implies that there is less active Na^+ loss and electrolyte disintegration to generate the solid electrolyte interphase for L-PFT at the initial stage. Furthermore, cycling instability of the S-PFT-based SMB is aggravated at high temperature (average Columbic efficiency ~ 99.24%), and the capacity retention is just 69.4% after 200 cycles at 0.5 C charge/1.0 C discharge in Fig. 3b. Instead, the L-PFT can support a higher CE of 99.63% and a very stable long cycling (capacity retention ~98.5%), indicating good performance at high-temperature for L-PFT.

XPS measurements were performed to further investigate the composition change of electrode surfaces as shown in Fig. 3c. Although the proportion of inorganic components (Na-F) in both L-PFT and S-LFT increased significantly compared to room temperature, the increase in S-LFT was more obvious. It is generally known that during the battery cycle, HF (mainly from $NaPF_6$ decomposition) will be produced at high temperatures, which will impair

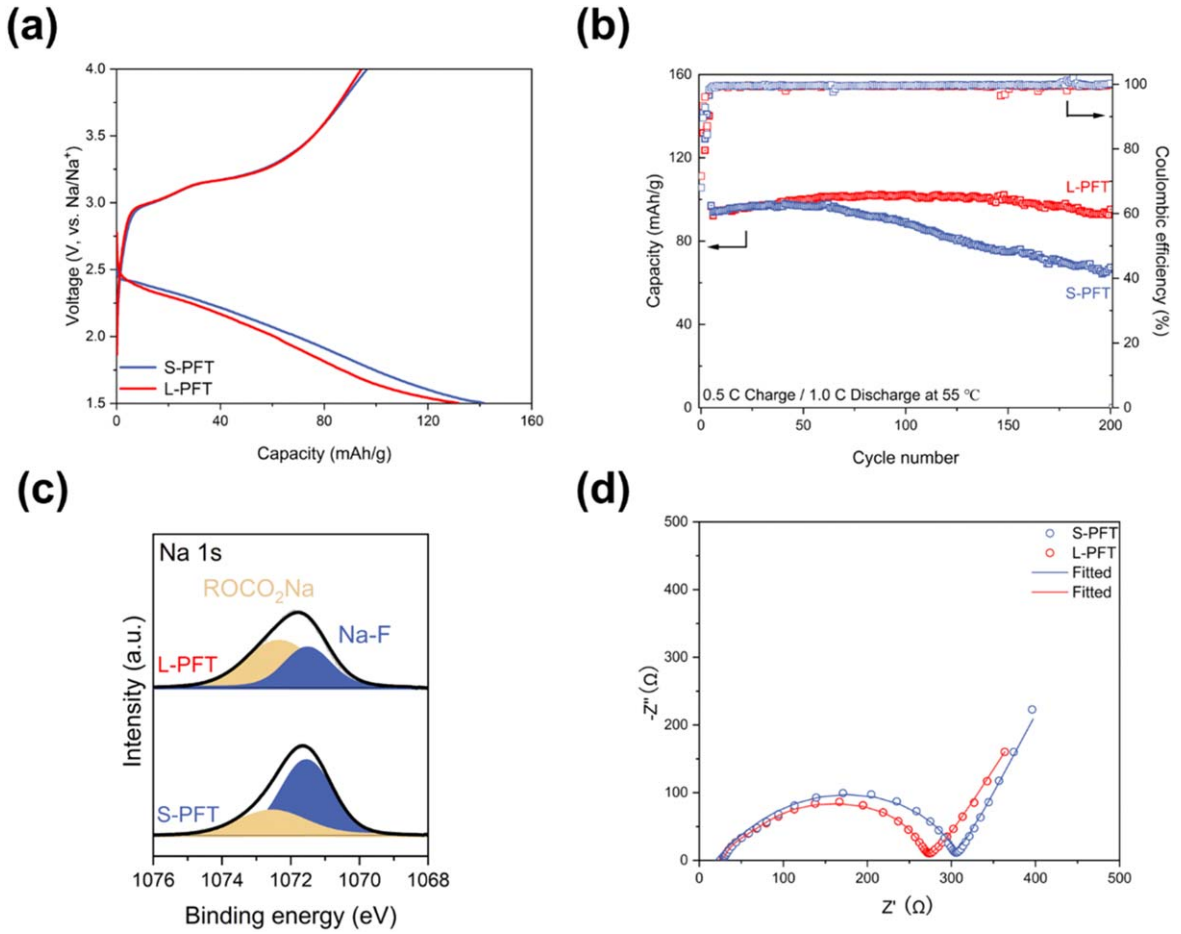

Figure 3. (a) Comparison for the initial cycle of L-PFT and S-PFT. (b) Cycling performance of the Na||$FePO_4$ cells with two electrolytes at 0.5 C charge/1.0 C discharge. (c) XPS spectra of cycled batteries: Na 1 s. (d) EIS results for S-PFT and L-PFT after long cycles.

battery stability.[31,34,35] This also explains why the capacity of a cell with L-PFT battery deteriorates at high operating temperature. EIS measurements following cycles of high temperatures are performed (see Fig. 3d). The S-PFT cell displays R_s (33.98 Ω). This resistance is marginally greater than that at room temperature, which can be related to the breakdown of sodium salt at elevated temperatures. Moreover, the constant breakdown of sodium salt raises the percentage of inorganic substances in the interphase, making it more prone to breakage. Repetitive breakdown and regeneration will cause the interphase's thickness to grow, consuming electrolytes and raising the interphase's impedance until it reaches 305.1 Ω (R_{cell}). In contrast, the degradation of sodium salt is limited when compared to L-PFT, and thus the impedance change is not as significant when compared to room temperature impedance (274.9 Ω). These results suggest thermodynamic stability issue is the key factor to be considered when the SMBs are at a high operating temperature.

Electrolyte performance at low temperature (−20 °C).—Given the low viscosity, high diffusion rate, and better wetting performance of the proposed L-PFT electrolyte, we expect SMB based on this electrolyte to perform well at low temperatures. The expectation was supported by our test of Na||$FePO_4$ system at −20 °C. As shown in Fig. 4a, the L-PFT battery performs well at low temperatures: it has an average CE of ∼99% within 300 cycles at 0.2 C. However, the S-PFT battery demonstrated a somewhat steady capacity of around 65 mAh g^{-1} in the initial 200 cycles. Following this, the capacity drastically decreased after 300 cycles. There exist several reasons for this decrease in capacity.

Firstly, while charging and discharging at low temperatures, sodium metal may easily precipitate on its surface. The precipitate will then react with the electrolyte to thicken the interphase film, hence raising the interface film's resistance.[36,37] Beyond the resistance temperature change in the interphase, there will also be a noticeable rise in the charge transfer impedance.[38] The EIS test demonstrates that the internal resistance rises above and that R_s is significantly greater at low temperatures than it is at room/high temperatures (see Fig. 4b). Moreover, scanning electron microscopy (SEM) was utilized to examine the morphology of the $FePO_4$ cathode after cycling. As depicted in Fig. S12, the surface of the $FePO_4$ cathode with S-PFT exhibited a porous and loose structure, which may contribute to increased resistance. In contrast, the cathode material in batteries with L-PFT demonstrated a relatively flat and densely packed surface morphology.

Additionally, when compared to the ratio at room temperature, we discovered that the SSIP ratio rose for both L-PFT and S-PFT, suggesting that the organic solvent phase is more tightly bound to sodium ions than the anion is (Figs. 4c and S13). Notably, MD results reveal that the SSIP ratio is highest in L-PFT, reaching 62.1%, compared to 42.5% observed in S-PFT. This ratio promotes the formation of an organic interphase, which lessens the metal expansion effect caused by the rise in sodium metal at low temperature.

Secondly, lattice shrinkage of the $FePO_4$ also contributes to the capacity decay observed, particularly at low temperatures. To investigate this, we used XRD to examine the cathodes after charging, as shown in Fig. 4d. The results reveal the presence of the $NaFePO_4$ phase in both the S-PFT and L-PFT electrolytes, with a higher fraction observed in S-PFT. This finding suggests that lattice shrinkage of the cathode material under low-temperature conditions hinders the complete extraction of Na^+ ions during charging.

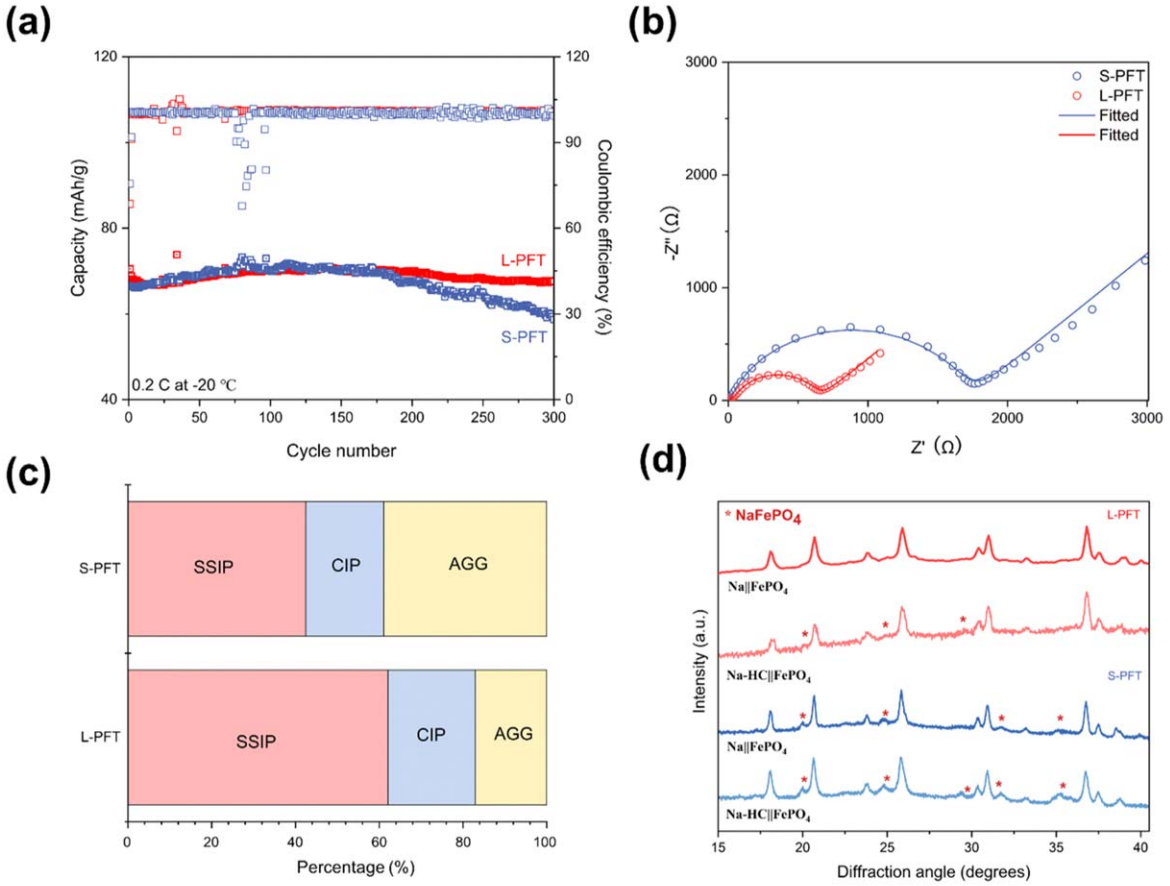

Figure 4. (a) Cycling performance of the Na||$FePO_4$ cells with two electrolytes at 0.2 C. (b) EIS results for S-PFT and L-PFT after long cycles. (c) Comparison for ratio of SSIP, CIP, and AGG for L-PFT and S-PFT. (d) XRD patterns of Na||$FePO_4$ and Na-HC||$FePO_4$ with two electrolytes after long cycles at low temperature.

Consequently, some sodium ions remain trapped in the cathode, further exacerbating the observed capacity decay. This behavior is more evident when Na-HC is used in place of sodium metal in full battery tests, as shown in Fig. S14. Specifically, Na-HC||$FePO_4$ full cells with the S-PFT electrolyte exhibit poor capacity retention of only ∼27% after 300 cycles. Moreover, a higher fraction of the $NaFePO_4$ phase is observed in full cells compared to half cells when using S-PFT. This indicates that the combination of Na-HC and the cathode material under low-temperature conditions exacerbates issues such as sodium ion trapping and incomplete extraction of Na^+ ions. These findings highlight the limitations of the electrolyte in supporting stable cycling, particularly in full-cell configurations.

Lastly, the reduction in conductivity, coupled with the increase in viscosity, is associated with the capacity decay (Fig. S15). The conductivity decreases from 3.83 mS cm^{-1} at room temperature to 2.84 mS cm^{-1} for L-PFT (3.61 mS cm^{-1}@S-PFT). The increase in intermolecular force causes viscosity to climb to 6.72 mPa·s for L-PFT. However, S-PFT has double the viscosity of L-PFT, measuring 12.72 mPa·s. These findings imply that when an SMB functions at a low temperature, the most important component to take into account is the physical and kinetic characteristics of the electrolyte itself.

Conclusions

In summary, our study demonstrates that sodium metal batteries (SMBs) can operate effectively with specifically designed low-concentration electrolytes, offering several unexpected advantages. In Na||$FePO_4$ cells, minimal capacity fading of approximately 0.02% per cycle was observed over 350 cycles at a 0.5 C charge/1 C discharge rate with L-PFT. Additionally, cells using L-PFT outperformed those with S-PFT at elevated temperatures (55 °C), exhibiting a higher Coulombic efficiency of 99.63% and stable long-term cycling with a capacity retention of around 98.5%. Moreover, the low viscosity, rapid ion diffusion, and enhanced wetting properties of L-PFT contributed to superior performance at low temperatures (−20 °C). These findings underscore the potential for developing high-performance SMBs through the strategic design of low-concentration electrolytes, which significantly reduces costs while maintaining robust performance across diverse temperatures.

Acknowledgments

The authors gratefully acknowledge the support from NSF under grant number 2208840 and the generous allocation of computing time by the ARC office at Virginia Tech.

ORCID

Qipeng Zhang https://orcid.org/0009-0009-1096-6267

References

1. P. K. Nayak, L. Yang, W. Brehm, and P. Adelhelm, "From lithium-ion to sodium-ion batteries: advantages, challenges, and surprises." *Angew. Chem. Int. Ed. Engl.*, **57**, 102 (2018).
2. C. Delmas, "Sodium and sodium-ion batteries: 50 Years of research." *Adv. Energy Mater.*, **8**, 1703137 (2018).
3. S-W. Kim, D-H. Seo, X. Ma, G. Ceder, and K. Kang, "Electrode materials for rechargeable sodium-ion batteries: potential alternatives to current lithium-ion batteries." *Adv. Energy Mater.*, **2**, 710 (2012).
4. J. Deng, W-B. Luo, S-L. Chou, H-K. Liu, and S-X. Dou, "Sodium-ion batteries: from academic research to practical commercialization." *Adv. Energy Mater.*, **8**, 1701428 (2018).
5. M. D. Slater, D. Kim, E. Lee, and C. S. Johnson, "Sodium-Ion batteries." *Adv. Funct. Mater.*, **23**, 947 (2013).

6. R. Usiskin, Y. Lu, J. Popovic, M. Law, P. Balaya, Y-S. Hu, and J. Maier, "Fundamentals, status and promise of sodium-based batteries." *Nat. Rev. Mater*, **6**, 1020–1035 (2021).
7. Y. Fang, X-Y. Yu, and X. W. Lou, "Nanostructured electrode materials for advanced sodium-ion batteries." *Matter*, **1**, 90 (2019).
8. H. Che, S. Chen, Y. Xie, H. Wang, K. Amine, X-Z. Liao, and Z-F. Ma, "Electrolyte design strategies and research progress for room-temperature sodium-ion batteries." *Energy Environ. Sci.*, **10**, 1075 (2017).
9. Y. Huang, L. Zhao, L. Li, M. Xie, F. Wu, and R. Chen, "Electrolytes and electrolyte/electrode interfaces in sodium-ion batteries: from scientific research to practical application." *Adv. Mater.*, **31**, e1808393 (2019).
10. M. Okoshi, Y. Yamada, S. Komaba, A. Yamada, and H. Nakai, "Theoretical analysis of interactions between potassium ions and organic electrolyte solvents: a comparison with lithium, sodium, and magnesium ions." *J. Electrochem. Soc.*, **164**, A54 (2016).
11. Y. Jin et al., "Highly reversible sodium ion batteries enabled by stable electrolyte-electrode interphases." *ACS Energy Lett.*, **5**, 3212 (2020).
12. H. Sun et al., "High-safety and high-energy-density lithium metal batteries in a novel ionic-liquid electrolyte." *Adv. Mater.*, **32**, e2001741 (2020).
13. X. Zheng, Z. Gu, X. Liu, Z. Wang, J. Wen, X. Wu, W. Luo, and Y. Huang, "Bridging the immiscibility of an all-fluoride fire extinguishant with highly-fluorinated electrolytes toward safe sodium metal batteries." *Energy Environ. Sci.*, **13**, 1788 (2020).
14. N. Wongittharom, T-C. Lee, C-H. Wang, Y-C. Wang, and J-K. Chang, "Electrochemical performance of Na/NaFePO4 sodium-ion batteries with ionic liquid electrolytes." *J. Mater. Chem. A*, **2**, 5655 (2014).
15. Y. Liu et al., "Weakly polar ether-aided ionic liquid electrolyte enables high-performance sodium metal batteries over wide temperature range." *Adv. Funct. Mater.*, **34**, 2312295 (2024).
16. J. Chen et al., "Nonflammable succinonitrile-based deep eutectic electrolyte for intrinsically safe high-voltage sodium-ion batteries." *Adv. Mater.*, **36**, e2400169 (2024).
17. S. Amara, J. Toulc'Hoat, L. Timperman, A. Biller, H. Galiano, C. Marcel, M. Ledigabel, and M. Anouti, "Comparative study of Alkali-Cation-Based (Li (+), Na(+), K(+)) electrolytes in acetonitrile and alkylcarbonates." *ChemPhysChem*, **20**, 581 (2019).
18. Y. Chen et al., "Trace ethylene carbonate-mediated low-concentration ether-based electrolytes for high-voltage lithium metal batteries." *Energy Environ. Sci.*, **17**, 5613 (2024).
19. X. Q. Zhang, X. B. Cheng, X. Chen, C. Yan, and Q. Zhang, "Fluoroethylene carbonate additives to render uniform Li deposits in lithium metal batteries." *Adv. Funct. Mater.*, **27**, 1605989 (2017).
20. E. Markevich, G. Salitra, F. Chesneau, M. Schmidt, and D. Aurbach, "Very stable lithium metal stripping–plating at a high rate and high areal capacity in fluoroethylene carbonate-based organic electrolyte solution." *ACS Energy Lett.*, **2**, 1321 (2017).
21. T. Jaumann et al., "Lifetime vs rate capability: understanding the role of FEC and VC in high-energy Li-ion batteries with nano-silicon anodes." *Energy Storage Mater.*, **6**, 26 (2017).
22. R. Holomb, W. Xu, H. Markusson, P. Johansson, and P. Jacobsson, "Vibrational spectroscopy and studies of Lithium Bis(oxalato)borate (LiBOB) in different Solvents." *J. Phys. Chem. A*, **110**, 11467 (2006).
23. Q. Zhang, N. Zhang, T. Yu, J. Zhang, B. Wen, and L. Zhang, "High-performance PEO-based solid-state $LiCoO_2$ lithium metal battery enabled by poly(acrylic acid) artificial cathode electrolyte interface." *Mater. Today Energy*, **29**, 101128 (2022).
24. L. Su, X. Zhao, M. Yi, H. Charalambous, H. Celio, Y. Liu, and A. Manthiram, "Uncovering the solvation structure of LiPF6-Based localized saturated electrolytes and their effect on $LiNiO_2$-based lithium-metal batteries." *Adv. Energy Mater.*, **12**, 2201911 (2022).
25. J. Moon, D. O. Kim, L. Bekaert, M. Song, J. Chung, D. Lee, A. Hubin, and J. Lim, "Non-fluorinated non-solvating cosolvent enabling superior performance of lithium metal negative electrode battery." *Nat. Commun.*, **13**, 4538 (2022).
26. T. Hou, K. D. Fong, J. Wang, and K. A. Persson, "The solvation structure, transport properties and reduction behavior of carbonate-based electrolytes of lithium-ion batteries." *Chem. Sci.*, **12**, 14740 (2021).
27. W. Tang et al., "High-performance $NaFePO_4$formed by aqueous ion-exchange and its mechanism for advanced sodium ion batteries." *J. Mater. Chem. A*, **4**, 4882 (2016).
28. Y. Fang, Q. Liu, L. Xiao, X. Ai, H. Yang, and Y. Cao, "High-performance olivine NaFePO4 microsphere cathode synthesized by aqueous electrochemical displacement method for sodium ion batteries." *ACS Appl. Mater. Interfaces*, **7**, 17977 (2015).
29. Y. Liu et al., "Electrolyte engineering with tamed electrode interphases for high-voltage sodium-ion batteries." *Adv. Mater.*, **36**, e2310051 (2024).
30. Q. Zhang, L. Bo, H. Li, L. Shen, J. Li, T. Li, Y. Xiao, Z. Tian, and Z. Li, "Inhibiting shuttle effect and dendrite growth in sodium-sulfur batteries enabled by applying external acoustic field." *Nano Lett.*, **24**, 10711 (2024).
31. F. Cheng, M. Cao, Q. Li, C. Fang, J. Han, and Y. Huang, "Electrolyte salts for sodium-ion batteries: NaPF(6) or NaClO(4)?" *ACS Nano*, **17**, 18608 (2023).
32. F. Huang, P. Xu, G. Fang, and S. Liang, "In-depth understanding of interfacial Na (+) behaviors in sodium metal anode: migration, desolvation, and deposition." *Adv. Mater.*, **36**, e2405310 (2024).
33. L. Zhu, Y. Li, J. Zhao, J. Liu, L. Wang, and J. Lei, "Recent advanced development of stabilizing sodium metal anodes." *Green Energy & Environment*, **8**, 1279 (2023).
34. Q. Li, Z. Cao, H. Cheng, J. Zhang, Z. Ma, W. Wahyudi, L. Cavallo, Q. Sun, and J. Ming, "Electrolyte boosting microdumbbell-structured alloy/metal oxide anode for fast-charging sodium-ion batteries." *ACS Materials Letters*, **4**, 2469 (2022).
35. G. Yan, K. Reeves, D. Foix, Z. Li, C. Cometto, S. Mariyappan, M. Salanne, and J. M. Tarascon, "A new electrolyte formulation for securing high temperature cycling and storage performances of Na-Ion batteries." *Adv. Energy Mater.*, **9**, 1901431 (2019).
36. C. Hu, S. Guo, F. Huang, Y. Yang, C. Yan, C. Z. Zhao, S. Liang, G. Fang, and Q. Zhang, "Carbonate ester-based sodium metal battery with high-capacity retention at -50 degrees C enabled by weak solvents and electrodeposited anode." *Angew. Chem. Int. Ed. Engl.*, **136**, e202407075 (2024).
37. C. Wang, A. C. Thenuwara, J. Luo, P. P. Shetty, M. T. McDowell, H. Zhu, S. Posada-Perez, H. Xiong, G. Hautier, and W. Li, "Extending the low-temperature operation of sodium metal batteries combining linear and cyclic ether-based electrolyte solutions." *Nat. Commun.*, **13**, 4934 (2022).
38. A. Huang, Z. Ma, P. Kumar, H. Liang, T. Cai, F. Zhao, Z. Cao, L. Cavallo, Q. Li, and J. Ming, "Low-temperature and fast-charging lithium metal batteries enabled by solvent-solvent interaction mediated electrolyte." *Nano Lett.*, **24**, 7499 (2024).